Chapter 5
Viscoelastic Lubrication Using the Second-Order Fluid

Alexandros T. Oratis, Vincent Bertin, Minkush Kansal, and Jacco H. Snoeijer

Abstract The classical theory of lubrication is dedicated to the flow of a viscous fluid in a narrow gap between two solid boundaries, with the specific goal of computing the resulting lubrication forces. These forces can be modified by elasticity: the solid boundary can deform elastically and/or the fluid can exhibit viscoelastic stress. Here we focus on the influence of elasticity inside the fluid, using the second-order fluid model, which for steady flows can be viewed as an expansion for small elasticity. We demonstrate how viscoelasticity changes the lubrication forces in various two-dimensional flow geometries, for which analytical solutions are presented. These examples illustrate the physical mechanisms of viscoelastic lubrication at small Deborah numbers. We also discuss the challenges of using the second-order fluid in unsteady flows and large Deborah numbers, and briefly comment on how the modelling framework can get extended to viscoelastic thin-film flows with free boundaries.

5.1 Introduction

Thin-film flows between solid surfaces can be found in a variety of biological, environmental, and engineering settings. These lubrication flows span significant length scales, ranging from kilometer-scale runaway landslides (Campbell, 1989), to the micrometer-scale motion of red blood cells in capillaries (Fitz-Gerald, 1969). Lubrication is crucial in the movement of synovial joints of mammals (Mow & Lai, 1979) and enhances the movement of machinery, such as gears and bearings (Hamrock et al., 2004). From a fundamental point of view, lubrication also plays a key role in determining the friction between two solid surfaces, and thus acts as important

We thank C. Datt and H. Stone for stimulating discussions. This work is supported by the N.W.O through the VICI Grant No. 680-47-632.

A. T. Oratis (✉) · V. Bertin · M. Kansal · J. H. Snoeijer
Physics of Fluids group, University of Twente, 7500 Enschede, AE, The Netherlands
e-mail: a.t.oratis@utwente.nl

B. Scheichl (ed.), *Interfacial Flows—The Power and Beauty of Asymptotic Methods*, CISM International Centre for Mechanical Sciences 615,
https://doi.org/10.1007/978-3-031-78764-5_5

tool in tribology (Veltkamp et al., 2021, 2023) and rheological measurements (Villey et al., 2013).

An extensive number of studies have been dedicated to understand fluid lubrication, since the pioneering study by Reynolds (Reynolds, 1886). An important feature of lubrication is the thin geometry along which the flow occurs, which enables a detailed analysis using a long-wave expansion. The flow induces a strong pressure in the liquid, which then exerts forces on the solid boundaries. Considering the sliding or rotating motion of two solid objects with symmetric profiles, the vertical lift force induced by the pressure vanishes for Newtonian lubrication with rigid boundaries. The pressure typically adopts a perfectly antisymmetric spatial profile, which when integrated along the sliding object's surface, leads to a zero lift. The absence of a lift force is a consequence of the reversibility of the Stokes equations. A way to generate lift forces is to introduce elasticity either in the solid boundary or the inside the liquid. As is sketched in Fig. 5.1, the elasticity indeed breaks the antisymmetry of the pressure. For instance, if the wall is soft, the lubrication pressure from a sliding cylinder parallel to a wall can cause elastic deformations (Fig. 5.1a). The coupling between the hydrodynamic lubrication with the elastic deformation leads to a pressure profile that causes a non-zero lift force on the cylinder (Sekimoto & Leibler, 1993; Skotheim & Mahadevan, 2004). The lift force on the object increases the liquid thickness, and thus allows for a fast translation past a deformable wall (Salez & Mahadevan, 2015; Saintyves et al., 2016). This subject of soft lubrication has thus been analyzed for various solid object geometries and motions (Jones et al., 2008; Martin et al., 2002; Mani et al., 2012; Pandey et al., 2016). Yet, another method to break the pressure antisymmetry is to consider to consider elasticity inside the lubricant, as can be the case for non-Newtonian liquids. Indeed, polymers dissolved in viscoelastic liquid can stretch with the flow and exert forces on the object arising from normal stress

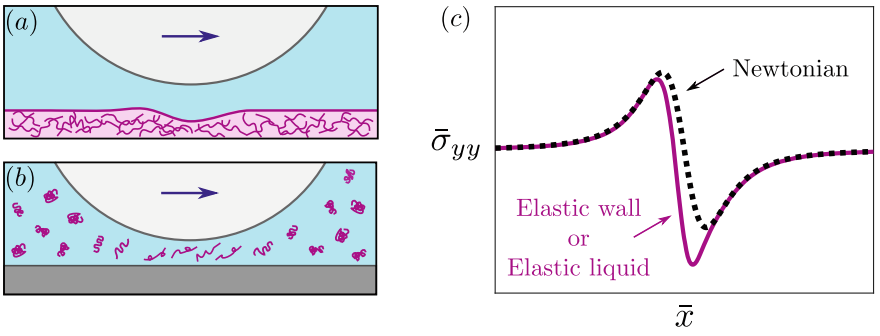

Fig. 5.1 Breaking the vertical stress anti-symmetry by introducing elasticity. **a** A cylinder sliding parallel to a soft wall induces an elastic deformation, which in turn pushes the cylinder upwards. **b** A cylinder sliding parallel to a wall in a viscoelastic liquid causes the dissolved polymers to stretch. **c** Vertical stress profiles σ_{yy} along the horizontal coordinate x. The elastic deformation of the soft wall or the polymer leads to breaking of the antisymmetry (solid line) compared to the Newtonian case

differences (Fig. 5.1b). The remaining question is to quantify how an elastic liquid can lead to a breaking of the stress antisymmetry similar to an elastic wall (Fig. 5.1c).

In this chapter, we revisit the effect of viscoelasticity on lubrication flows. Incorporating viscoelasticity in lubrication equations via long-wave expansions of constitutive models is a difficult task. One possible way to overcome this challenge is to consider the second-order fluid model, which expresses the stress tensor in powers of the velocity gradient (Bird et al., 1987; Tanner, 2000). The advantage of the second-order fluid is that it provides exact expressions for the normal stress differences by only having to solve the equivalent Newtonian problem. Using the so-called Tanner's theorem, one can obtain analytical expressions for the liquid pressure and stresses without having to solve the flow field of the full viscoelastic problem (Tanner, 2000). Owing to its simplicity, it has been used to study several creeping flows (Ardekani et al., 2008; Leal, 1975; Phillips, 1996; Vishnampet & Saintillan, 2012), and in particular lubrication problems, such as the sliding motion of bearings (Bourgin, 1982; Huang et al., 2002; Sawyer & Tichy, 1998), the sedimentation of solid particles (Cao et al., 2022; Hu & Joseph, 1999), and the squeeze flow between two plates (Brindley et al., 1976). However, the second-order fluid has its limitations and can lead to unphysical predictions of lubrication flows. For instance, it does not predict stress relaxation and is thus invalid for highly unsteady flows, such as squeezing (Morozov & Spagnolie, 2015). Furthermore, because the second-order fluid is itself an expansion about the Newtonian fluid, it is valid only for weakly viscoelastic flows. Yet, in the limit of weak and steady viscoelastic flows, even the more sophisticated upper convected Maxwell or the Giesekus models yield the same results as the second-order fluid in the limit of small Deborah numbers (De Corato et al., 2016). We thus proceed with the second-order fluid, as it still offers the simplest constitutive relation that admits normal stress differences, and for which exact results can be computed for lubrication forces. We highlight several features induced by normal stresses, such as the ability to produce extra lift and the role of pressure variations across the gap (absent in the Newtonian limit).

5.2 Governing Equations and Tanner's Theorem

We study the two-dimensional flow generated by an object moving close to a solid wall, using a Cartesian coordinate system $\hat{\mathbf{e}}_x, \hat{\mathbf{e}}_y$ (Fig. 5.2). The vertical gap $h(x, t)$ between the object and wall can vary along the horizontal coordinate x and time t. The inertia of the fluid is assumed to be negligible, such that the fluid flow is described by the mass and momentum conservation

$$\boldsymbol{\nabla} \cdot \mathbf{u} = 0, \tag{5.1}$$

$$\boldsymbol{\nabla} \cdot \boldsymbol{\sigma} = \mathbf{0}. \tag{5.2}$$

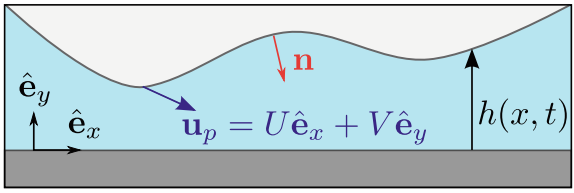

Fig. 5.2 Schematic illustrating the narrow liquid gap with thickness $h(x,t)$ formed between the solid wall and the moving object. The velocity of the sliding object is $\mathbf{u}_p = U\hat{\mathbf{e}}_x + V\hat{\mathbf{e}}_y$ and its unit normal is defined as $\mathbf{n}$

Here $\mathbf{u} = u\hat{\mathbf{e}}_x + v\hat{\mathbf{e}}_y$ is the fluid velocity, and $\boldsymbol{\sigma} = -p\mathbf{I} + \boldsymbol{\tau}$ the stress tensor, which consists of an isotropic pressure p and a deviatoric stress $\boldsymbol{\tau}$. For the second-order fluid, the deviatoric stress can be written as

$$\boldsymbol{\tau} = \eta\dot{\boldsymbol{\gamma}} - \frac{\psi_1}{2}\overset{\triangledown}{\dot{\boldsymbol{\gamma}}} + \psi_2\dot{\boldsymbol{\gamma}}\cdot\dot{\boldsymbol{\gamma}}, \tag{5.3}$$

where first term corresponds to the contribution due to the fluid's viscosity η, while the remaining two terms are the viscoelastic contributions. The parameters ψ_1 and ψ_2 denote the first and second normal stress coefficients. The rate of strain tensor is defined as $\dot{\boldsymbol{\gamma}} = \boldsymbol{\nabla}\mathbf{u} + (\boldsymbol{\nabla}\mathbf{u})^{\mathrm{T}}$, with $(\boldsymbol{\nabla}\mathbf{u})_{ij} = \partial u_j/\partial x_i$, and the upper convected derivative as

$$\overset{\triangledown}{\dot{\boldsymbol{\gamma}}} = \frac{\mathrm{d}\dot{\boldsymbol{\gamma}}}{\mathrm{d}t} - (\nabla\mathbf{u})^{\mathrm{T}}\cdot\dot{\boldsymbol{\gamma}} - \dot{\boldsymbol{\gamma}}\cdot\nabla\mathbf{u}. \tag{5.4}$$

We employ no-slip boundary conditions at the wall and the object such that

$$\mathbf{u} = \mathbf{0} \quad \text{at} \quad y = 0, \tag{5.5}$$

$$\mathbf{u} = \mathbf{u}_p = U\hat{\mathbf{e}}_x + V\hat{\mathbf{e}}_y \quad \text{at} \quad y = h(x,t), \tag{5.6}$$

where U and V are, respectively, the horizontal and vertical components of the object's velocity (Fig. 5.2). Finally, the mass conservation together with the kinematic boundary condition give

$$\frac{\partial h}{\partial t} + \frac{\partial}{\partial x}\int_0^{h(x,t)} u\,\mathrm{d}y = 0. \tag{5.7}$$

Importantly, for a second-order fluid satisfying a two-dimensional Stokes flow, we can apply Tanner's theorem, which significantly simplifies the analysis (Bird et al., 1987; Tanner, 2000). This theorem states that for a problem described by velocity boundary conditions, the velocity field does not differ from the Newtonian version of the same problem, but the pressure is modified to

$$p = p_N - \frac{\psi_1}{2\eta}\frac{\mathrm{D}p_N}{\mathrm{D}t} + \left(\frac{\psi_1}{8} + \frac{\psi_2}{2}\right)(\dot{\boldsymbol{\gamma}} : \dot{\boldsymbol{\gamma}}), \tag{5.8}$$

where p_N is the pressure of the Newtonian problem satisfying $\boldsymbol{\nabla} p_N = \eta \nabla^2 \mathbf{u}$ with the same boundary conditions. Thus, by solving the Newtonian problem in terms of the velocity gradient and pressure, we can use Tanner's theorem to determine the viscoelastic pressure, and by extension, the viscoelastic stresses. We note that Tanner's theorem is valid only for two-dimensional plane flows with velocity boundary conditions (e.g. no slip, imposed flux, rigid boundaries). The theorem can be extended for three-dimensional flows only when $\psi_2 = -\psi_1/2$ (Bird et al., 1987).

5.3 Lubrication Approximation

We now turn to the lubrication approximation for thin gaps. We first recall the relevant length scales involved in Newtonian lubrication, which lead to the two-dimensional lubrication equation. We then incorporate the viscoelastic effects of the second-order fluid via Tanner's theorem. For completion, we also present the lubrication approximation by performing a long-wave expansion of the momentum and constitutive relations. The resulting equations offer an alternate route for dealing with viscoelastic lubrication problems without having to invoke Tanner's theorem.

5.3.1 Relevant Scales and Newtonian Lubrication

Given the characteristic horizontal and vertical length scales ℓ and h_0 respectively, we can define the parameter $\epsilon = h_0/\ell \ll 1$, which is small for slender films. We non-dimensionalize the variables of interest using the following relations

$$\begin{aligned} &\bar{x} = \frac{x}{\ell}, \quad \bar{y} = \frac{y}{h_0}, \quad \bar{u} = \frac{u}{U}, \quad \bar{v} = \frac{v}{\epsilon U}, \quad \bar{t} = \frac{Ut}{\ell} \\ &\bar{h}(\bar{x}, \bar{t}) = \frac{h(x,t)}{h_0}, \quad \bar{p} = \frac{h_0^2}{\eta U \ell} p. \end{aligned} \tag{5.9}$$

The lubrication equations are obtained by expanding the flow quantities in powers of ϵ, such that $\{\bar{u}, \bar{v}, \bar{p}\} = \{\bar{u}_0, \bar{v}_0, \bar{p}_0\} + \epsilon\{\bar{u}_1, \bar{v}_1, \bar{p}_1\} + \mathcal{O}(\epsilon^2)$. We start by considering the Newtonian problem and neglect any viscoelastic contributions. Retaining only the leading order terms and re-dimensionalizing, the Stokes equations (5.2) in the lubrication approximation become

$$\frac{\partial p_N}{\partial x} = \eta \frac{\partial^2 u}{\partial y^2}, \tag{5.10}$$

$$\frac{\partial p_N}{\partial y} = 0. \tag{5.11}$$

The pressure does not vary across the liquid gap in the y-direction, which is a hallmark of Newtonian lubrication flows. When we apply the no-slip boundary conditions, the velocity takes the form

$$u(x, y, t) = \frac{1}{2\eta}\frac{\partial p_N}{\partial x}(y^2 - yh) + \frac{Uy}{h}, \tag{5.12}$$

which consists of a parabolic Poiseuille flow and a linear Couette flow. Integrating across the film to obtain the flux, the kinematic boundary condition (5.7) reduces to the Reynold's equation

$$\frac{\partial h}{\partial t} - \frac{\partial}{\partial x}\left(\frac{h^3}{12\eta}\frac{\partial p_N}{\partial x} - \frac{Uh}{2}\right) = 0. \tag{5.13}$$

Thus, for a given thickness profile, one can solve for the pressure using (5.13) and, by extension, the velocity using (5.12). The resulting pressure can be used to compute the lift.

5.3.2 *Viscoelastic Lubrication Version 1: Tanner's Theorem*

For the second-order fluid, we can access the relevant stresses in the problem by applying Tanner's theorem. Rather than performing a long-wave expansion of the momentum and constitutive equations, we only need to expand the pressure about its Newtonian value, as given in (5.8). Using the scales from (5.9), the leading order viscoelastic pressure reads

$$p = p_N - \frac{\psi_1}{2\eta}\left(\frac{\partial p_N}{\partial t} + u\frac{\partial p_N}{\partial x}\right) + \left(\frac{\psi_1}{4} + \psi_2\right)\left(\frac{\partial u}{\partial y}\right)^2. \tag{5.14}$$

We note that the pressure depends on the velocity, u, and the dominant shear rate, $\partial u/\partial y$, both of which vary strongly across the film. Moreover, the Newtonian pressure p_N is given by (5.13). Thus, unlike Newtonian lubrication where the pressure remains uniform across the film thickness, the pressure for the second-order fluid has a non-trivial y-dependence. With this expression for the pressure we can now compute the leading order terms for each component of the stress tensor, which give

$$\sigma_{xx} = -p_N + \frac{\psi_1}{2\eta}\left(\frac{\partial p_N}{\partial t} + u\frac{\partial p_N}{\partial x}\right) + \frac{3\psi_1}{4}\left(\frac{\partial u}{\partial y}\right)^2, \tag{5.15}$$

$$\sigma_{yy} = -p_N + \frac{\psi_1}{2\eta}\left(\frac{\partial p_N}{\partial t} + u\frac{\partial p_N}{\partial x}\right) - \frac{\psi_1}{4}\left(\frac{\partial u}{\partial y}\right)^2, \tag{5.16}$$

$$\sigma_{xy} = \eta\frac{\partial u}{\partial y} - \frac{\psi_1}{2}\left[\frac{\partial}{\partial t}\left(\frac{\partial u}{\partial y}\right) + u\frac{\partial^2 u}{\partial x \partial y} + v\frac{\partial^2 u}{\partial y^2} + 2\frac{\partial u}{\partial x}\frac{\partial u}{\partial y}\right]. \tag{5.17}$$

Even though the second normal stress coefficient ψ_2 appears in the pressure, it completely disappears from every component of the stress tensor $\boldsymbol{\sigma}$ (Joseph & Feng, 1996). Taking the normal stress difference we get the expected result

$$\sigma_{xx} - \sigma_{yy} = \psi_1\left(\frac{\partial u}{\partial y}\right)^2. \tag{5.18}$$

Note that the expressions for the stresses (5.15)–(5.17) are obtained using only the scales introduced in (5.9). They are independent of boundary conditions or the equations presented in Sect. 5.3.1. Therefore, these stress expressions exhibit Galilean invariance and are independent of the reference frame. This invariance will prove quite useful when we consider objects sliding parallel to a wall in the following sections.

Since, unlike the Newtonian case, the stress is not uniform across the gap, we can make the y-dependence of the stress tensor explicit by substituting the velocity (5.12) in the expressions above. It turns out that only one component of the stress turns out homogeneous across the gap, namely σ_{yy}. The explicit form reads

$$\sigma_{yy} = -p_N + \frac{\psi_1}{2\eta}\frac{\partial p_N}{\partial t} - \frac{\psi_1}{4}\left[\frac{1}{2\eta}\frac{\partial p_N}{\partial x}h - \frac{U}{h}\right]^2, \tag{5.19}$$

which, is indeed independent of y, since $p_N = p_N(x,t)$. By virtue of (5.18) it then follows that σ_{xx} has an extra term $\psi_1\left(\frac{\partial u}{\partial y}\right)^2$, and therefore σ_{xx}, in general, will exhibit a y-dependence. It is also of interest to consider the corresponding expression for the pressure, which after substitution of (5.12) takes the form

$$p = p_N - \frac{\psi_1}{2\eta}\frac{\partial p_N}{\partial t} + \frac{\psi_1}{4}\left[\frac{1}{2\eta}\frac{\partial p_N}{\partial x}h - \frac{U}{h}\right]^2 + \psi_2\left[\frac{1}{2\eta}\frac{\partial p_N}{\partial x}(2y-h) - \frac{U}{h}\right]^2. \tag{5.20}$$

The contribution of ψ_1 is homogeneous across the gap, while there is an inhomogeneity associated to ψ_2. We recall that the total stress tensor $\boldsymbol{\sigma}$ turns out independent of ψ_2; its appearance in p will be cancelled by the contribution from the deviatoric $\boldsymbol{\tau}$ and is thus of limited physical importance. A similar expression for the viscoelastic pressure can be computed using a formal long-wave expansion of the full problem, as is shown in the next subsection.

5.3.3 Viscoelastic Lubrication Version 2: Long-Wave Expansion

We close this section by presenting the long-wave expansion of the lubrication flows using the second-order fluid, without invoking Tanner's theorem. The analysis is adapted from Datt et al. (2022). Implementing the scales introduced in (5.9), the leading order stress components can be reduced to

$$\sigma_{xx} = -p + (\psi_1 + \psi_2)\left(\frac{\partial u}{\partial y}\right)^2, \tag{5.21}$$

$$\sigma_{yy} = -p + \psi_2\left(\frac{\partial u}{\partial y}\right)^2, \tag{5.22}$$

$$\sigma_{xy} = \eta\frac{\partial u}{\partial y} - \frac{\psi_1}{2}\left[\frac{\partial}{\partial t}\left(\frac{\partial u}{\partial y}\right) + u\frac{\partial^2 u}{\partial x \partial y} + v\frac{\partial^2 u}{\partial y^2} - 2\frac{\partial u}{\partial y}\frac{\partial v}{\partial y}\right]. \tag{5.23}$$

The resulting Stokes equations then become

$$\frac{\partial p}{\partial x} = \eta\frac{\partial^2 u}{\partial y^2} - \frac{\psi_1}{2}\mathcal{N}(u, v) + \psi_2\frac{\partial}{\partial x}\left[\left(\frac{\partial u}{\partial y}\right)^2\right], \tag{5.24}$$

$$\frac{\partial p}{\partial y} = \psi_2\frac{\partial}{\partial y}\left[\left(\frac{\partial u}{\partial y}\right)^2\right], \tag{5.25}$$

where we have introduced a non-linear operator

$$\mathcal{N}(u, v) = \frac{\partial}{\partial t}\left(\frac{\partial^2 u}{\partial y^2}\right) + v\frac{\partial^3 u}{\partial y^3} + \frac{\partial}{\partial x}\left[u\frac{\partial^2 u}{\partial y^2} - \frac{1}{2}\left(\frac{\partial u}{\partial y}\right)^2\right]. \tag{5.26}$$

Equation (5.11) indicates that the pressure will vary across the gap, unless $\psi_2 = 0$, consistent with the result from (5.20). To further investigate how the viscoelastic contributions in (5.24) and (5.25) affect the pressure, it is instructive to introduce a modified pressure p_{m} (Datt et al., 2022), defined as

$$p_{\mathrm{m}} = p + \frac{\psi_1}{2}\left[u\frac{\partial^2 u}{\partial y^2} - \frac{1}{2}\left(\frac{\partial u}{\partial y}\right)^2\right] - \psi_2\left(\frac{\partial u}{\partial y}\right)^2. \tag{5.27}$$

Using the modified pressure, the momentum equations can be significantly simplified to

$$\frac{\partial p_{\mathrm{m}}}{\partial x} = \left(\eta - \frac{\psi_1}{2}\frac{\partial}{\partial t}\right)\left(\frac{\partial^2 u}{\partial y^2}\right) - \frac{\psi_1}{2} v \frac{\partial^3 u}{\partial y^3}, \tag{5.28}$$

$$\frac{\partial p_{\mathrm{m}}}{\partial y} = \psi_2 u \left(\frac{\partial^3 u}{\partial y^3}\right). \tag{5.29}$$

We note that the Newtonian-like structure of (5.10) and (5.11) is recovered when $\partial^3 u/\partial y^3 = 0$. We therefore look for a parabolic structure of the velocity profile

$$u(x, y, t) = -\frac{A(x,t)}{2}(y^2 - yh) + \frac{Uy}{h}, \tag{5.30}$$

which satisfies the no-slip boundary conditions (5.5) and (5.6). Here, $A(x, t)$ reflects the strength of the parabolic flow and in the limit of a Newtonian liquid it is equivalent to minus the pressure gradient over the viscosity. From the kinematic boundary condition (5.7), we can obtain an evolution equation relating the flow strength $A(x, t)$ to the geometry of the lubrication film $h(x, t)$, which becomes

$$\frac{\partial h}{\partial t} + \frac{\partial}{\partial x}\left(\frac{Ah^3}{12} + \frac{Uh}{2}\right) = 0. \tag{5.31}$$

Comparing (5.31) with (5.13), we can interpret the flow strength $A(x, t)$ in terms of the Newtonian pressure via the connection $A = -\frac{\partial p_N}{\partial x}/\eta$. From (5.29) it follows that a parabolic velocity profile leads to a uniform modified pressure across the film. Consequently, the modified pressure can be determined by the horizontal momentum balance (5.28), which simplifies to

$$\frac{\partial p_{\mathrm{m}}}{\partial x} = -\left(\eta - \frac{\psi_1}{2}\frac{\partial}{\partial t}\right) A(x, t). \tag{5.32}$$

Finally, the modified pressure can be related back to the actual pressure using (5.27)

$$p(x, t) = p_{\mathrm{m}}(x, t) + \frac{\psi_1}{4}\left[\frac{Ah}{2} + \frac{U}{h}\right]^2 + \psi_2\left[-\frac{A}{2}(2y - h) + \frac{U}{h}\right]^2. \tag{5.33}$$

Equations (5.30)–(5.33) can be used to analyze various lubrication problems involving the second-order fluid. We note that upon replacing $A(x, t)$ with $-\frac{\partial p_N}{\partial x}/\eta$ in (5.32) we can solve for p_{m} by integrating along x. Injecting the modified pressure in (5.33), we recover an equation identical to Tanner's theorem (5.20). Therefore, in the remainder of this chapter, we shall use the results from Tanner's theorem to compute the pressure and stresses for each problem of interest.

5.4 Applications

5.4.1 *Pressure Drop Along a Channel*

We contextualize Tanner's theorem for two-dimensional viscoelastic flows by applying it to various lubrication problems, starting with the flow along a narrow channel of varying thickness $h(x)$ and length ℓ (Fig. 5.3). The inlet and outlet of the channel are set at $x = 0$ and $x = \ell$ respectively. Our goal is to determine the viscoelastic effects on the pressure drop along the channel, given an imposed constant flux $q = \int_0^{h(x)} u \, \mathrm{d}y$. This problem was recently addressed by Boyko and Stone, using the reciprocal theorem (Boyko & Stone, 2021). Here, we re-examine this problem using the formalism developed in Sect. 5.3. From (5.12) and (5.13) we know that the solution to the Newtonian problem is given by

$$\frac{\partial p_N}{\partial x} = -\frac{12\eta q}{h^3}, \tag{5.34}$$

$$u(x, y) = -\frac{6q}{h^3}(y^2 - yh). \tag{5.35}$$

Using Tanner's theorem for lubrication flows (5.14), we can directly solve for the pressure, which becomes

$$p(x, y) = p_N(x) + 9\psi_1 \left(\frac{q}{h^2}\right)^2 \left[4\frac{\psi_2}{\psi_1}\left(\frac{2y}{h} - 1\right)^2 + 1\right]. \tag{5.36}$$

The term q/h^2 represents a characteristic shear rate, such that the viscoelastic contribution to the pressure drop can be interpreted as a normal stress difference given in (5.18). Interestingly, we find that the pressure does not remain uniform across the channel, and has a y-dependence through the second normal stress coefficient ψ_2. This finding cannot be captured by the reciprocal theorem, as the y-dependence does not allow for the required integration of the pressure across the channel walls. Yet, setting $\psi_2 = 0$, we recover a pressure drop relation that agrees with the result obtained by Boyko and Stone under the same assumption. As anticipated from (5.15),

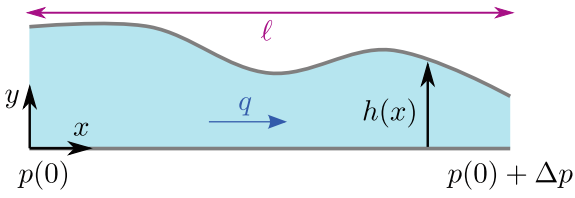

Fig. 5.3 Schematic of a channel with length ℓ and varying thickness $h(x)$. The imposed flux q causes a pressure drop Δp along the channel

the viscoelastic contribution to the horizontal fluid stress resisting the flow depends on y but not on ψ_2

$$\sigma_{xx} = -p_N + 9\psi_1 \left(\frac{q}{h}\right)^2 \left[2\left(\frac{2y}{h} - 1\right)^2 + 1\right]. \tag{5.37}$$

For Newtonian lubrication flows, the pressure drop and horizontal stress decrease and increase, respectively, along the direction of the flow. This dependence of the direction is rooted in the fact that both quantities have a linear dependence on the velocity. In contrast, the pressure and stress for viscoelastic lubrication flows involve a quadratic dependence on the velocity. As a result, the viscoelastic contribution to these quantities is independent of the flow direction. Furthermore, we notice that only the profile of the channel $h(x)$ dictates the extra pressure drop and stress (Boyko & Stone, 2021).

5.4.2 *Lift on a Sliding Object*

We continue by considering the vertical lift force exerted on an object sliding parallel to a solid wall, such that $V = 0$ (see Fig. 5.2). It is more convenient to switch to the frame of reference of the moving object with a shifted horizontal coordinate $\tilde{x} = x - Ut$. Using this reference frame, the thickness becomes time-independent and varies only spatially $h(x, t) = h(\tilde{x})$. As a result, the problem becomes steady and we can remove the time derivatives in (5.13)–(5.17). The boundary conditions for the horizontal velocity at the wall and at the object transform to $u(\tilde{x}, 0) = -U$ and $u(\tilde{x}, h(\tilde{x})) = 0$ (see Fig. 5.2). Given the unit normal on the object $\mathbf{n} \approx h'(\tilde{x})\hat{\mathbf{e}}_x - \hat{\mathbf{e}}_y$ (see Fig. 5.2), the lift (per unit length), to leading order, can be expressed

$$\mathcal{L} = \hat{\mathbf{e}}_y \cdot \int \mathbf{n} \cdot \boldsymbol{\sigma} \, \mathrm{d}\mathcal{S} = -\int_{-\infty}^{\infty} \sigma_{yy}\big|_{y=h(\tilde{x})} \, \mathrm{d}x. \tag{5.38}$$

Since we are considering the co-moving frame of the object, the flow is steady making the stress σ_{yy} in (5.16) simpler to evaluate. Indeed, the first viscoelastic term in (5.16) vanishes for steady flows ($\partial p_N/\partial t = 0$). Moreover, at $y = h(\tilde{x})$ we have $u = 0$, such that the second viscoelastic term also cancels. Thus, the lift on the object simplifies to

$$\mathcal{L} = \mathcal{L}_N + \frac{\psi_1}{4} \int_{-\infty}^{\infty} \left(\frac{\partial u}{\partial y}\right)^2 \Bigg|_{y=h(\tilde{x})} \mathrm{d}x, \tag{5.39}$$

where $\mathcal{L}_N \equiv \int_{-\infty}^{\infty} p_N \, \mathrm{d}x$ is the lift force of the Newtonian problem. The normal stress effect provided by the second-order fluid induces an extra lift on the object. Once

the spatial profile $h(x)$ is specified, one can compute the shear rate using (5.12) and evaluate explicitly the viscoelastic correction. Note that (5.39) is the same expression obtained by Tanner when considering the force exerted on a tilted plate sliding next to a solid wall (Tanner, 2000); however, the expression is valid for arbitrary shapes of the lubricated gap $h(\tilde{x})$. We shall now revisit the tilted plate-slider as well as the lift on cylindrical objects to obtain exact expressions for the viscoelastic lift contributions.

Flat plate We first consider the sliding motion of a tilted flat plate. The profile of the film thickness varies linearly in space $h(\tilde{x}) = h_1 + \alpha\tilde{x}$. The slope of the plate $\alpha = (h_2 - h_1)/\ell$ depends on the inlet and outlet thickness h_1 and h_2 respectively, and the horizontal span of the plate ℓ (see Fig. 5.4a). For the lubrication equations to be valid, we require $\alpha \ll 1$. This example is a textbook lubrication problem (Batchelor, 1967; Tanner, 2000), as the pressure buildup in the film induces a lift force $\mathcal{L}$ on the plate for $h_1 < h(\tilde{x}) < h_2$. Our goal here is to determine the viscoelastic correction to the lift. We first solve for the Newtonian pressure using (5.13)

$$p_N(\tilde{x}) = p_0 + \frac{6\eta U}{\alpha(h_2 + h_1)}\left(-1 + \frac{h_1 + h_2}{h(\tilde{x})} - \frac{h_1 h_2}{h(\tilde{x})^2}\right), \tag{5.40}$$

and recall that the velocity remains the same as the Newtonian problem given by (5.12), which yields

$$u(\tilde{x}, y) = U\left(\frac{y}{h(\tilde{x})} - 1\right)\left(\frac{6y}{h(\tilde{x})^2}\frac{h_1 h_2}{h_1 + h_2} - \frac{3y}{h(\tilde{x})} + 1\right). \tag{5.41}$$

To arrive at this pressure and velocity profile, we have assumed that the pressure at the ends of the plate reaches the ambient pressure p_0. The pressure profile becomes asymmetric, with the degree of asymmetry depending on the slope of the plate (see bottom of Fig. 5.4a). From the pressure and velocity profiles we can evaluate the Newtonian and viscoelastic contributions to the lift in (5.39), which become

$$\begin{aligned}\mathcal{L} = {} & \frac{6\eta U}{\alpha^2}\left[\ln\left(\frac{h_2}{h_1}\right) - \frac{2(h_2 - h_1)}{h_2 + h_1}\right] \\ & + \frac{\psi_1 U^2}{\alpha}\frac{h_2 - h_1}{(h_2 + h_1)^2}\left[\frac{h_1}{h_2} + \frac{h_2}{h_1} - 1\right].\end{aligned} \tag{5.42}$$

The first term corresponds to the standard Newtonian lift and scales as α^{-2}. Because this result is valid only in the limit of small slopes $\alpha \ll 1$, we anticipate the viscoelastic effects to be a small correction to the Newtonian lift. Indeed, the second-order fluid is predicated on the assumption of a small Deborah number, $\mathrm{De} \equiv \psi_1 U/(2\eta\ell) \ll 1$, and hence leads to lift of order $O(\alpha)$ smaller than the Newtonian contribution. The effect will be more dramatic for symmetric sliders, as will be clear below.

Cylinder We next examine the motion of a cylinder with radius R moving next to the wall at a vertical distance h_0 (see Fig. 5.4b). This example has similar features as the cylinder sliding next to a soft wall discussed in Sect. 5.1 (see Fig. 5.1). In the frame

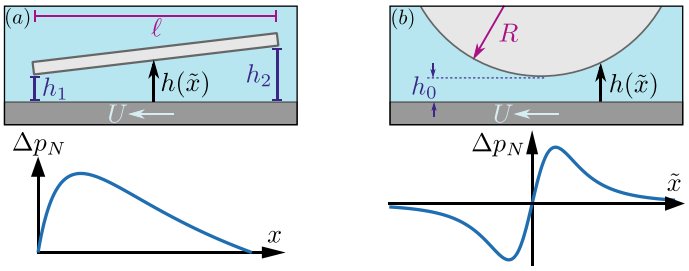

Fig. 5.4 Horizontal sliding with respect to a wall moving with velocity U. **a** Cartoon schematic of an inclined flat plate with thickness $h(\tilde{x}) = h_1 + (h_2 - h_1)\tilde{x}/\ell$ and spanning a horizontal distance ℓ (Top). The Newtonian pressure Δp_N profile along the film position x becomes asymmetric for sufficiently small ratios $m = h_1/h_2$ (Bottom). **b** Cartoon schematic of the cylinder with radius R forming a nearly parabolic film with thickness $h(\tilde{x})$ (Top). The bottom of the cylinder is separated from the wall by distance h_0. The pressure profile becomes antisymmetric with respect to the center of the cylinder (Bottom)

of reference of the cylinder, the wall is moving with velocity $-U$. The lubrication film between wall and cylinder adopts a nearly parabolic shape at the bottom of the cylinder

$$h(\tilde{x}) \approx h_0 \left(1 + \frac{\tilde{x}^2}{2Rh_0}\right). \tag{5.43}$$

The pressure for a Newtonian liquid gives a profile (Jeffrey & Onishi, 1981)

$$p_N(\tilde{x}) = p_0 + \frac{2\eta U\tilde{x}}{h(\tilde{x})^2}, \tag{5.44}$$

which is antisymmetric with respect to the center of the cylinder (see Fig. 5.4b). Thus, the Newtonian lift obtained from integrating the pressure is zero, causing no vertical force on the cylinder. Yet, the normal stress differences break the antisymmetry and lead to a non-zero force. The pressure profile leads to a velocity

$$u(\tilde{x}, y) = U\left(\frac{y}{h(\tilde{x})} - 1\right)\left[\frac{yh_0}{h(\tilde{x})^2}\left(4 - 3\frac{h(\tilde{x})}{h_0}\right) + 1\right], \tag{5.45}$$

which can be used to determine the shear rate on the plate. Combining the shear rate with the thickness profile in (5.39), we can compute the lift exerted on the cylinder, which becomes

$$\mathcal{L} = \frac{\pi}{2\sqrt{2}} \frac{\psi_1 U^2 R^{1/2}}{h_0^{3/2}}. \tag{5.46}$$

As anticipated, the lift for both the slider and cylinder scales with the typical normal stress difference $\psi_1(U/h)^2$ integrated over a length ℓ, which scales as $\ell \sim h/\alpha$ and $\ell \sim (hR)^{1/2}$ for the slider and cylinder respectively.

Hence, we see a fundamental difference in the role of the viscoelastic stress in the two examples. In the case of the slider, the lift produced by the normal stress difference complements the viscous lift but is only a small correction. In contrast, the symmetry of the sliding cylinder leads to zero lift when surrounded by a Newtonian liquid. The lift induced by the viscoelastic stress is thus the sole contribution to the vertical force experienced by the cylinder.

5.4.3 Drag on a Sliding Object

Thus far we have only focused on the vertical forces exerted on the sliding object. We now turn our attention to the viscoelastic effects on the horizontal drag force. Using the unit normal, one can evaluate the drag on the object as

$$\mathcal{D} = \hat{\mathbf{e}}_x \cdot \int \mathbf{n} \cdot \boldsymbol{\sigma} \mathrm{d}\mathcal{S} = \int_{-\infty}^{\infty} \left(h'(\tilde{x})\sigma_{xx} - \sigma_{xy} \right)\big|_{y=h(\tilde{x})} \, \mathrm{d}x = -\int_{-\infty}^{\infty} \sigma_{xy}\big|_{y=0} \, \mathrm{d}x. \tag{5.47}$$

The last equality arises from Newton's third law, such that the drag on the object is equal and opposite to the drag on the wall, $y = 0$, which is easier to evaluate. Indeed, using (5.17) we see that for $y = 0$, the last two viscoelastic terms in the shear stress vanish, since $v = 0$ and $\partial u/\partial x = 0$. The first viscoelastic term also vanishes for steady flows, leaving only one viscoelastic contribution to the drag

$$\begin{aligned} \mathcal{D} &= -\int_{-\infty}^{\infty} \left[\eta \frac{\partial u}{\partial y} - \frac{\psi_1 u}{2} \frac{\partial^2 u}{\partial x \partial y} \right]\Bigg|_{y=0} \mathrm{d}x \\ &= \mathcal{D}_N - \frac{\psi_1 U}{2} \left(\left. \frac{\partial u}{\partial y} \right|_{y=0} \right)\Bigg|_{x\to-\infty}^{x\to\infty}, \end{aligned} \tag{5.48}$$

where $\mathcal{D}_N \equiv \int_{-\infty}^{\infty} \eta(\partial u/\partial y)|_{y=0} \, \mathrm{d}x$ is the drag of the Newtonian problem. Importantly, the drag $\mathcal{D}$ vanishes in certain situations depending on the boundary conditions of the shear rate at the far field. For symmetric objects, the shear rate is identical at the two extreme ends and thus viscoelasticity does not alter the drag. Similarly, for objects whose profiles diverge at far-field, the shear rate is zero at the two extremes. Therefore, within the second-order fluid, viscoelasticity will affect the drag only for asymmetric objects, whose films at the two ends have a finite thickness.

Returning to the example of the flat plate, we anticipate a non-zero drag due to the asymmetry the thin film forms with the wall. Making use of (5.41) and (5.48) we find that the drag becomes

$$\mathcal{D} = \frac{2\eta U}{\alpha} \left[2 \ln\left(\frac{h_1}{h_2} \right) + \frac{3(h_2 - h_1)}{h_1 + h_2} \right] - \psi_1 U^2 \left(\frac{1}{h_1} - \frac{1}{h_2} \right), \tag{5.49}$$

which is smaller than the Newtonian drag for $h_1 < h_2$. Considering the small tilt angles $\alpha \ll 1$ for which this expression is valid, we find again that the viscoelastic correction is by an order $O(\alpha)$ smaller than the Newtonian drag.

5.4.4 Unsteady Lift Force

All the examples we have analyzed up to this point involved steady flows. As an example of an unsteady flow, we consider the vertical sedimentation of a flat plate towards a wall where the thickness of the film varies with time (see Fig. 5.5a). Consequently, the time derivative in (5.16) is no longer zero and the lift on the falling object consists of an additional term

$$\mathcal{L} = \mathcal{L}_N + \psi_1 \int_{-\infty}^{\infty} \left[\frac{1}{4} \left(\frac{\partial u}{\partial y} \right)^2 \Bigg|_{y=h(\tilde{x})} - \frac{1}{2\eta} \frac{\partial p_N}{\partial t} \right] \mathrm{d}x. \tag{5.50}$$

Solving first for the pressure and the velocity of the Newtonian problem using (5.13) and (5.12), we arrive at

$$p_N(x) = p_0 + \frac{6\eta \dot{h} \ell^2}{h^3} \left(\frac{x^2}{\ell^2} - \frac{x}{\ell} \right), \tag{5.51}$$

and

$$u(x, y) = \frac{3\dot{h}\ell}{h} \left(\frac{2x}{\ell} - 1 \right) \left(\frac{y^2}{h^2} - \frac{y}{h} \right). \tag{5.52}$$

The pressure in the Newtonian problem adopts a parabolic shape, with a maximum pressure at the center of the plate (see Fig. 5.5a). Injecting the velocity and pressure profiles into (5.50), the lift becomes

$$\mathcal{L}(t) = -\frac{\eta \ell^3 \dot{h}}{h^3} + \frac{\psi_1 \ell^3}{2} \left(\frac{\ddot{h}}{h^3} - \frac{3\dot{h}^2}{2h^4} \right). \tag{5.53}$$

The first term corresponds to the viscous force, whereas the remaining two terms are the viscoelastic contributions. We first note that the negative sign of the normal stress difference term $\psi_1 \dot{h}^2 \ell^3 / h^4$, which promotes the attraction of the plate to the wall, regardless of the direction of motion. The second noteworthy result is that the other viscoelastic term involves the acceleration of the plate $\ddot{h}$. Bearing in mind that ψ_1 is to be taken positive, this acceleration term has the same effect as a negative mass—providing a highly unsteady, unphysical feedback on the dynamical equation for $h(t)$. This reflects that the second-order fluid is not suited for highly unsteady flows.

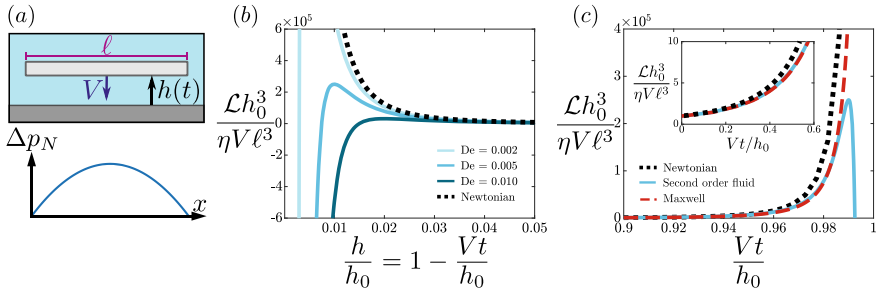

Fig. 5.5 Prediction of the second-order fluid in unsteady flows. **a** For a flat plate with length ℓ translating towards a wall with speed V (top), the Newtonian pressure Δp_N adopts a spatially parabolic profile (bottom). **b** For a Newtonian liquid, the normalized lift force $\mathcal{L}h_0^3/(\eta V \ell^3)$ diverges as the thickness decreases (dotted line). Introducing viscoelasticity with the second-order fluid, the lift force is non-monotonic and becomes negative once the plate has reaches a critical thickness. The critical thickness at which this transition occurs increases with the Deborah number $\mathrm{De} = \lambda V/h_0$ (solid lines). **c** Equivalently, the normalized lift force diverges as time increases for a Newtonian liquid. Similarly, the lift force for a Maxwell model also diverges but is smaller than the Newtonian lift for $\mathrm{De} = 0.005$. The lift force for Maxwell and second-order fluid agree well at early times (inset), before it starts decreasing for the second-order fluid

To avoid the issue of the acceleration term, we restrict ourselves to the case where the plate moves downward with a constant speed V. The film thickness decreases linearly with time $h(t) = h_0 - Vt$, where h_0 is an initial thickness. Because the acceleration term drops, the remaining viscoelastic and viscous terms give rise to an unsteady lift fore $\mathcal{L}(t)$ that depends only on the gap thickness $h(t)$, which satisfies the following dimensionless equation:

$$\frac{\mathcal{L}h_0^3}{\eta V \ell^3} = \left(\frac{h_0}{h}\right)^3 - \mathrm{De}\left(\frac{h_0}{h}\right)^4. \tag{5.54}$$

We have introduced the initial gap thickness h_0 and the Deborah number $\mathrm{De} = \psi_1 V/(2\eta\epsilon\ell) = \psi_1 V/(2\eta h_0)$, where $\epsilon = h_0/\ell$ is the initial aspect ratio of the film. For a Newtonian liquid the lift force diverges with the film thickness as $\mathcal{L} \sim 1/h^3$ (dotted line in Fig. 5.5b). To test the effects of the second-order fluid, we overlay the prediction of Eq. (5.53) for different values of De. When the plate is sufficiently far away from the wall, the prediction between Newtonian and second-order fluid are almost identical. However, as the plate gets closer to the wall, the viscoelastic force overcomes the viscous force, and leads to a negative lift (solid lines in Fig. 5.5b). Because the viscoelastic force is negative, it generates an extra force that pulls the plate towards the wall instead of pushing it. The stronger the degree of viscoelasticity, the sooner the lift deviates from the Newtonian behavior. From (5.54), we find that the transition from the repulsion to attraction in the lift occurs when the thickness reaches a value $h = \mathrm{De}h_0$.

Bearing in mind the limitations of the second-order model for unsteady flows, we also discuss a different estimate of the viscoelastic lift, via the linear Maxwell model. This linear model is valid only for small deformations, i.e. h close to h_0, but is able to capture unsteady effects. Using the lubrication approach described in Tanner (2000), the lift force then satisfies

$$\left(1+\lambda\frac{\partial}{\partial t}\right)\mathcal{L}=-\frac{\eta\ell^3\dot{h}}{h^3}, \tag{5.55}$$

with λ being the relaxation time of the liquid and is related to the normal stress difference coefficient through $\lambda=\psi_1/(2\eta)$. The Deborah number can be expressed with the relaxation time via $\mathrm{De}=\lambda V/h_0$. The lift force predicted by the linear Maxwell liquid continues to grow indefinitely, slightly slower than the Newtonian lift (dashed line in Fig. 5.5c). The lift from (5.54) agrees very well with the Maxwell prediction up to the point where it starts decreasing. This simple example illustrates how the linear Maxwell model provides much better estimates for very fast and unsteady flows. Unlike the second-order fluid, the Maxwell liquid exhibits "stress memory", where the stress relaxes with the relaxation time λ. Conversely, the linear Maxwell model is limited to small deformations and fails to capture effects arising from normal stress differences, which are linked to large deformations and are inherently nonlinear. Indeed, considering the steady flows described earlier, the linear Maxwell liquid would not lead to any viscoelastic contributions to the lift on the plate or cylinder. One can overcome this limitation with the upper convected Maxwell model, which involves both normal stress effects and stress relaxation (Phan-Thien & Tanner, 1983; Tichy, 1996).

5.5 Conclusion and Outlook

In this chapter we employed the second-order fluid to investigate viscoelastic effects in lubrication flows arising in objects with rigid boundaries. Specifically, for the two-dimensional geometries we considered we were able to utilize Tanner's theorem, which allowed for a direct calculation of the pressures and stresses by only having to solve for the equivalent Newtonian problems. Following the work done by previous studies (Joseph & Feng, 1996; Tanner, 2000), Tanner's theorem indicates that the pressure has a non-trivial y-dependence through the second normal stress difference coefficient ψ_2. Conversely, ψ_2 does not appear in any stress component and, furthermore, the vertical stress component σ_{yy} does not depend on y. These local stresses allowed us to make predictions for global quantities, such the pressure drop in a channel or the lift and drag forces on sliding objects.

Our analysis shows that the normal stress differences lead to an enhanced lift for a cylinder sliding parallel to a wall. This result supports previously published numerical findings on sliding cylinders, even at moderate Deborah numbers (Feng et al., 1996; Singh & Joseph, 2000). An enhanced lift can also be extended to sliding spheres

using the second- and third-order fluid models (Becker et al., 1996; Hu & Joseph, 1999). However, the lift enhancement on spheres is not supported by numerical and experimental investigations, which instead show that the sphere tends to be attracted towards the wall (Becker et al., 1996; Feng et al., 1996; Joseph et al., 1994; Singh & Joseph, 2000). This discrepancy may stem from the drastically different Deborah numbers in each respective system. The second order fluid is an expansion about the Newtonian fluid and is thus valid only for weakly viscoelastic flows at small Deborah numbers. Conversely, the reduced lift reported by experiments and numerical simulations was found at moderate Deborah numbers. Why the lift gets enhanced for cylinders but reduced for spheres at large Deborah numbers remains an open question.

Unlike the enhancement of the lift, the second-order fluid does not influence the drag unless the sliding object has an asymmetric profile. The absence of a viscoelastic contribution to the drag can be simply seen by reversing the flow direction, which would lead to the same direction for the lift but opposite direction for the drag. Because, the normal stress differences scale with U^2, they contribute to the lift but not to the drag. In our analysis we mainly considered the second-order fluid, which consists of only the first expansion of the stress in terms of the Deborah number. We thus expect a correction to the drag for strongly viscoelastic flows, which would involve expanding to higher orders of the Deborah number. Such an expansion would lead to odd powers of the velocity, such that the flow reversal argument is still fulfilled. Indeed, this situation resembles the drag past an unconstrained sphere in a viscoelastic liquid (Leslie & Tanner, 1961). The drag corrections only manifest in even powers of the Deborah number, and thus odd powers of the velocity (Faroughi et al., 2020; Housiadas & Tanner, 2016).

As a perspective we conclude by discussing how the analysis employed can be adapted to interfacial flows of thin liquid films. A key element of the analysis above is that the flow geometry is externally imposed for rigid boundaries. This is no longer the case for liquid films that are bounded from above by a free surface; in fact, we are interested in computing how normal stresses modify the shape of the interface. The application of Tanner's theorem is thus not straightforward, and one relies on the formal long-wave expansion of the system (see Sect. 5.3.3). We recently carried out this expansion (Datt et al., 2022), leading to a velocity that still exhibits a "Poiseuille" structure in the vertical direction,

$$\frac{\partial h}{\partial t} + \frac{1}{3}\frac{\partial}{\partial x}\left(Ah^3\right) = 0, \tag{5.56}$$

very much like the Newtonian case. Importantly, however, the flow strength $A(x, t)$ is governed by an auxiliary equation that accounts for viscoelastic effects:

$$\gamma\frac{\partial^3 h}{\partial x^3} - \eta A + \frac{\psi_1}{2}\left[\frac{\partial A}{\partial t} + \frac{1}{2}\frac{\partial}{\partial x}\left(A^2h^2\right)\right] = 0. \tag{5.57}$$

This indeed offers a framework for viscoelastic thin films, based on the second-order fluid. Apart from the interplay between viscous and viscoelastic forces, this equation also considers capillary effects through the surface tension γ. A few observations are in order. First, for $\psi_1 = 0$ one recovers the usual viscous thin film equation via $\eta A = \gamma \partial^3 h / \partial x^3$. Second, the equations do not invoke ψ_2, i.e. the second normal stress difference does not play any role in the analysis of capillary stress. This is in line with the observation that for rigid boundaries the stress only involves ψ_1. Third, flows that are steady in a moving frame (like in dip-coating), the fields are travelling waves of the form $A(\tilde{x}), h(\tilde{x})$, with $\tilde{x} = x - Ut$; in this case $A(\tilde{x})$ can be eliminated, to yield a single, autonomous equation for $h(\tilde{x})$. Recent applications covered the steady wetting flows encountered for dip-coating (Landau-Levich-Derjaguin problem) and moving contact lines (Kansal et al., 2024). Though one should bear in mind the limitations of the second-order fluid, many further extensions can be envisioned based on the proposed viscoelastic thin film framework.

References

Ardekani, A. M., Rangel, R. H., Joseph, D. D. (2008) Two spheres in a free stream of a second-order fluid. *Physics of Fluids, 20*(6).

Batchelor, G. K. (1967). *An introduction to fluid dynamics*. Cambridge university Press.

Becker, L. E., McKinley, G. H., & Stone, H. A. (1996). Sedimentation of a sphere near a plane wall: weak non-newtonian and inertial effects. *Journal of Non-Newtonian Fluid Mechanics, 63*(2–3), 201–233.

Bird, R. B., Armstrong, R. C., & Hassager, O. (1987). *Dynamics of polymeric liquids. Vol. 1: Fluid mechanics*.

Bourgin, P. (1982). Second order effects in non-newtonian lubrication theory. a general perturbation approach. *The Journal of Lubrication Technology, 104*, 547–552.

Boyko, E., & Stone, H. A. (2021). Reciprocal theorem for calculating the flow rate-pressure drop relation for complex fluids in narrow geometries. *Physical Review Fluids, 6*(8), L081301.

Brindley, G., Davies, J. M., & Walters, K. (1976). Elastico-viscous squeeze films. part i. *Journal of Non-Newtonian Fluid Mechanics,1*(1), 19–37.

Campbell, C. S. (1989). Self-lubrication for long runout landslides. *The Journal of Geology, 97*(6), 653–665.

Cao, D., Dvoriashyna, M., Liu, S., Lauga, E., & Wu, Y. (2022). Reduced surface accumulation of swimming bacteria in viscoelastic polymer fluids. *Proceedings of the National Academy of Sciences, 119*(45), e2212078119.

Datt, C., Kansal, M., & Snoeijer, J. H. (2022). A thin-film equation for a viscoelastic fluid, and its application to the landau-levich problem. *Journal of Non-Newtonian Fluid Mechanics, 305*, 104816.

De Corato, M., Greco, F., & Maffettone, P. L. (2016). Reply to "comment on 'locomotion of a microorganism in weakly viscoelastic liquids"'. *Physical Review E, 94*(5), 057102.

Faroughi, S. A., Fernandes, C., Nóbrega, J. M., & McKinley, G. H. (2020). A closure model for the drag coefficient of a sphere translating in a viscoelastic fluid. *Journal of Non-Newtonian Fluid Mechanics, 277*, 104218.

Feng, J., Huang, P. Y., & Joseph, D. D. (1996). Dynamic simulation of sedimentation of solid particles in an oldroyd-b fluid. *Journal of Non-Newtonian Fluid Mechanics, 63*(1), 63–88.

Fitz-Gerald, J. M. (1969). Mechanics of red-cell motion through very narrow capillaries. *Proceedings of the Royal Society B, 174*(1035), 193–227.

Hamrock, B. J., Schmid, S. R., Jacobson, B. O. (2004). *Fundamentals of fluid film lubrication*. CRC Press.

Housiadas, K. D., & Tanner, R. I. (2016). A high-order perturbation solution for the steady sedimentation of a sphere in a viscoelastic fluid. *Journal of Non-Newtonian Fluid Mechanics, 233*, 166–180.

Hu, H. H., & Joseph, D. D. (1999). Lift on a sphere near a plane wall in a second-order fluid. *Journal of Non-Newtonian Fluid Mechanics, 88*(1–2), 173–184.

Huang, P., Li, Z., Meng, Y., & Wen, S. (2002). Study on thin film lubrication with second-order fluid. *Journal of Tribology, 124*(3), 547–552.

Jeffrey, D. J., & Onishi, Y. (1981). The slow motion of a cylinder next to a plane wall. *The Quarterly Journal of Mechanics and Applied Mathematics, 34*(2), 129–137.

Jones, M. B., Fulford, G. R., Please, C. P., McElwain, D. L. S., & Collins, M. J. (2008). Elastohydrodynamics of the eyelid wiper. *Bulletin of Mathematical Biology, 70*, 323–343.

Joseph, D. D., & Feng, J. (1996). A note on the forces that move particles in a second-order fluid. *Journal of Non-Newtonian Fluid Mechanics, 64*(2–3), 299–302.

Joseph, D. D., Liu, Y. J., Poletto, M., & Feng, J. (1994). Aggregation and dispersion of spheres falling in viscoelastic liquids. *Journal of Non-Newtonian Fluid Mechanics, 54*, 45–86.

Kansal, M., Bertin, V., Datt, C., Eggers, J., & Snoeijer, J. H. (2024). Viscoelastic wetting: Cox-voinov theory with normal stress effects. *Journal of Fluid Mechanics*, *985*, A17.

Leal, L. G. (1975). The slow motion of slender rod-like particles in a second-order fluid. *Journal of Fluid Mechanics, 69*(2), 305–337.

Leslie, F. M., & Tanner, R. I. (1961). The slow flow of a visco-elastic liquid past a sphere. *The Quarterly Journal of Mechanics and Applied Mathematics, 14*(1), 36–48.

Mani, M., Gopinath, A., & Mahadevan, L. (2012). How things get stuck: kinetics, elastohydrodynamics, and soft adhesion. *Physical Review Letters, 108*(22), 226104.

Martin, A., Clain, J., Buguin, A., & Brochard-Wyart, F. (2002). Wetting transitions at soft, sliding interfaces. *Physical Review E, 65*(3), 031605.

Morozov, A., Spagnolie, S. E. (2015). Introduction to complex fluids. *Complex Fluids in Biological Systems: Experiment, Theory, and Computation,* 3–52.

Mow, V. C., & Lai, W. M. (1979). Mechanics of animal joints. *Annual Review of Fluid Mechanics, 11*(1), 247–288.

Pandey, A., Karpitschka, S., Venner, C. H., & Snoeijer, J. H. (2016). Lubrication of soft viscoelastic solids. *Journal of Fluid Mechanics, 799*, 433–447.

Phan-Thien, N., & Tanner, R. I. (1983). Viscoelastic squeeze-film flows-maxwell fluids. *Journal of Fluid Mechanics, 129*, 265–281.

Phillips, R. J. (1996). Dynamic simulation of hydrodynamically interacting spheres in a quiescent second-order fluid. *Journal of Fluid Mechanics, 315*, 345–365.

Reynolds, O. (1886). Iv. On the theory of lubrication and its application to Mr. Beauchamp tower's experiments, including an experimental determination of the viscosity of olive oil. *Philosophical Transactions of the Royal Society,* (177), 157–234.

Saintyves, B., Jules, T., Salez, T., & Mahadevan, L. (2016). Self-sustained lift and low friction via soft lubrication. *Proceedings of the National Academy of Sciences, 113*(21), 5847–5849.

Salez, T., & Mahadevan, L. (2015). Elastohydrodynamics of a sliding, spinning and sedimenting cylinder near a soft wall. *Journal of Fluid Mechanics, 779*, 181–196.

Sawyer, W. G., & Tichy, J. A. (1998). Non-newtonian lubrication with the second-order fluid. *Journal of Tribology, 120*, 622–628.

Sekimoto, K., & Leibler, L. (1993). A mechanism for shear thickening of polymer-bearing surfaces: elasto-hydrodynamic coupling. *EPL, 23*(2), 113.

Singh, P., & Joseph, D. D. (2000). Sedimentation of a sphere near a vertical wall in an oldroyd-b fluid. *Journal of Non-Newtonian Fluid Mechanics, 94*(2–3), 179–203.

Skotheim, J. M., & Mahadevan, L. (2004). Soft lubrication. *Physical Review Letters, 92*(24), 245509.

Tanner, R. I. (2000). *Engineering rheology* (Vol. 52). OUP Oxford.

Tichy, J. A. (1996). Non-newtonian lubrication with the convected maxwell model. *Transactions of the ASME Journal of Tribology, 118*, 344–348.

Veltkamp, B., Jagielka, J., Velikov, K. P., & Bonn, D. (2023). Lubrication with non-newtonian fluids. *Physical Review Applied, 19*(1), 014056.

Veltkamp, B., Velikov, K. P., Venner, C. H., & Bonn, D. (2021). Lubricated friction and the hersey number. *Physical Review Letters, 126*(4), 044301.

Villey, R., Martinot, E., Cottin-Bizonne, C., Phaner-Goutorbe, M., Léger, L., Restagno, F., & Charlaix, E. (2013). Effect of surface elasticity on the rheology of nanometric liquids. *Physical Review Letters, 111*(21), 215701.

Vishnampet, R., & Saintillan, D. (2012). Concentration instability of sedimenting spheres in a second-order fluid. *Physics of Fluids, 24*(7), 073302.